⌘ *Author's Choice*

THE JOURNAL OF BIOLOGICAL CHEMISTRY VOL. 286, NO. 24, pp. 21755–21766, June 17, 2011
Printed in the U.S.A.

Drosophila melanogaster Myosin-18 Represents a Highly Divergent Motor with Actin Tethering Properties*

Received for publication, January 4, 2011, and in revised form, April 8, 2011 Published, JBC Papers in Press, April 17, 2011, DOI 10.1074/jbc.M111.218669

Stephanie Guzik-Lendrum[‡§], Attila Nagy[‡], Yasuharu Takagi[‡], Anne Houdusse[¶], and James R. Sellers[‡1]

From the [‡]Laboratory of Molecular Physiology, NHLBI, National Institutes of Health, Bethesda, Maryland 20892, [§]Department of Cell and Developmental Biology, University of North Carolina, Chapel Hill, North Carolina 27599, and [¶]Structural Motility, Institut Curie CNRS, UMR144, 26 rue d'Ulm, 75248 Paris Cedex 05, France

The gene encoding *Drosophila* myosin-18 is complex and can potentially yield six alternatively spliced mRNAs. One of the major features of this myosin is an N-terminal PDZ domain that is included in some of the predicted alternatively spliced products. To explore the biochemical properties of this protein, we engineered two minimal motor domain (MMD)-like constructs, one that contains the N-terminal PDZ (myosin-18 M-PDZ) domain and one that does not (myosin-18 M-ΔPDZ). These two constructs were expressed in the baculovirus/Sf9 system. The results suggest that *Drosophila* myosin-18 is highly divergent from most other myosins in the superfamily. Neither of the MMD constructs had an actin-activated MgATPase activity, nor did they even bind ATP. Both myosin-18 M-PDZ and M-ΔPDZ proteins bound to actin with K_d values of 2.61 and 1.04 μM, respectively, but only about 50–75% of the protein bound to actin even at high actin concentrations. Unbound proteins from these actin binding assays reiterated the 60% saturation maximum, suggesting an equilibrium between actin-binding and non-actin-binding conformations of *Drosophila* myosin-18 *in vitro*. Neither the binding affinity nor the substoichiometric binding was significantly affected by ATP. Optical trapping of single molecules in three-bead assays showed short lived interactions of the myosin-18 motors with actin filaments. Combined, these data suggest that this highly divergent motor may function as an actin tethering protein.

The myosin superfamily is composed of 36 known classes of molecular motor proteins based on amino acid sequence homology (1). In general, myosins are characterized by a catalytic motor domain responsible for binding actin and hydrolyzing ATP. Despite high amino acid sequence homologies in the motor domains, there is considerable variation in the enzymatic and mechanical properties of myosins that allows for the performance of widely different tasks within cells.

The founding member of class 18 of the myosin superfamily, originally called MysPDZ and later myosin-18A, was distinguished from other myosin classes by the presence of a PDZ domain located upstream of the motor domain (2). PDZ domains are protein-interacting modules that are common components of proteins that establish and maintain molecular complexes within the cell, such as scaffolding proteins involved in cellular signaling cascades (3). N-terminal PDZ domains within the myosin superfamily are specific to class 18 (1). There is also a lysine and glutamic acid (KE)-rich sequence in mammalian myosin-18A that lies at the extreme N terminus followed by a short amino acid sequence between this domain and the PDZ domain. Both the PDZ domain and the KE-rich domain are missing in some alternatively spliced isoforms of mammalian myosin-18A.

Mammals express another myosin-18 isoform (termed myosin-18B), which is encoded by a unique gene (4, 5). This myosin is missing the PDZ domain. A gene in *Drosophila melanogaster* for myosin-18 was identified through genome sequence analyses searching for myosin motor domains (6, 7). Since its initial identification as a possible myosin, no analyses on *Drosophila* myosin-18 have been published.

The amino acid sequences of myosin-18 isoforms reveal the presence of a consensus IQ motif that might be expected to bind calmodulin or a calmodulin family member, such as the regulatory or essential light chains. It also has a long tail region that is predicted to form an extended, but interrupted, coiled coil domain, which should serve to dimerize the molecule. In this regard, the myosin-18 has some similarities to class 2 myosins (8). Whether myosin-18 molecules can self-associate to form filaments via this tail is an open question.

Class 18 myosins in mice and humans have been implicated in physiological events, including stromal cell differentiation (18A) (2) and tumor suppression (18B) (4, 9, 10). In mammalian cell culture, myosin-18A has been suggested to play a role in maintenance of trans-Golgi structure and maintenance of actin networks in the lamellipodia (11, 12). However, a biochemical analysis on murine myosin-18A suggested that its actin binding properties are markedly different from previously described myosins. There is an ATP-insensitive actin binding site located in the KE region or the region in between the KE region and the PDZ domain (13). Furthermore, the isoform lacking the KE region does not appear to bind actin even in the absence of ATP (13, 14).

In this study, we expressed *Drosophila* myosin-18 motor domain-containing fragments in an Sf9/baculoviral system for biochemical analysis. We show that this myosin motor does not bind ATP, but unlike the mammalian myosin-18A, the core motor domain does bind actin. This suggests a role for *Drosophila* myosin-18 as a dynamic actin tether.

* This work was supported, in whole or in part, by National Institutes of Health intramural funds from the NHLBI.

⌘ *Author's Choice*—Final version full access.

[1] To whom correspondence should be addressed. Tel.: 301-496-6887; Fax: 301-402-1519; E-mail: sellersj@nhlbi.nih.gov.

EXPERIMENTAL PROCEDURES

Sequence Analysis of Drosophila Myosin-18—Exon analysis and sequence alignment of all six isoforms CG31045 (the gene annotation for *Drosophila* Mhcl from FlyBase) against the reverse complement of the full genomic sequence of *D. melanogaster* chromosome 3R (GenBank™ accession number AE014297.2) were performed using ClustalW (European Molecular Biology Laboratory).

5′ Rapid Amplification of cDNA Ends—Full-length sequences of CG31045-A and -F were isolated through 5′ RACE[2] using mRNA isolated from whole fly using a TRIzol extraction protocol (15). A cDNA pool was generated by reverse transcription PCR using oligo(dT) primers and SuperScript II reverse transcriptase (Invitrogen). Sequences were amplified from cDNA with Platinum HiFi Supermix (Invitrogen) and standard PCR techniques (PTC-200 Thermocycler, MJ Research). 5′ RACE primary amplification was performed with the primer pair downstream primer (1856A) CGGAACATGGAGACAACCTT and upstream Universal Anchor Primer (Invitrogen) CUACUACUACUAGGCCACGCGTCGACTAGTACGGGIIGGGIIGGGIIG followed by nested amplification with the primer pair downstream primer CTGCTTCTCGACATCGTCCT (1665A, 954F) and upstream Abridged Universal Anchor Primer (Invitrogen) CUACUACUACUAGGCCACG CGTCGACTAGTAC.

Antibody Production and Embryo Staining—A polyclonal genomic antibody was generated in rabbit and affinity-purified with ELISA against *Drosophila* myosin-18 amino acids Val^{1913}–Ile^{2012} (Isoform A; Val^{1676}–Ile^{1775} in Isoform F) in the coiled coil region of the protein (Strategic Diagnostics Inc., Newark, DE). *Drosophila* embryos were collected, fixed, and stained using protocols by Harlow and Lane (16, 17) with the exceptions that 4% paraformaldehyde solution in PBS was used in place of PIPES-buffered formaldehyde solution for fixation and that all wash steps during the staining procedure were done over a period of 30 min using PBS containing 1% Triton X-100. Embryos were stained with the primary antibody at a 1:1,000 dilution in blocking buffer and with secondary Alexa Fluor 488 goat anti-rabbit antibody (Invitrogen, Molecular Probes) at 1:5,000 in blocking buffer. Stained embryos were stored in Vectashield antifade mounting medium (Vector Laboratories, Inc., Burlingame, CA). Confocal microscopy was performed using a Zeiss LSM 510 confocal system with a 20×, 0.75 numerical aperture oil immersion objective and 488 nm laser excitation using a depth of 1.2 μm per section. For illustrating the ubiquitous nature of the staining, 17 confocal sections were projected into a single image.

PCR Amplification and Cloning of Drosophila Myosin-18—Cloning of myosin-18 utilized aforementioned cDNA pools and primer pairs designed to amplify and ligate 5′ and 3′ halves of the sequence as follows: 5′ sequence of CG31045-A (1–5130): upstream primer, ATTATCGGTCCGATGTTCAACTTTATGAA; downstream primer, CTTGGCTTGTTCGAGCACTGTATCTGAC; 3′ sequence of CG31045-A (4173–6125): upstream primer, CAACGAGATGAACGATCTGCGCATG; downstream primer, AATTAACTAGTCGATACTTGGCGTTATTT; 5′ sequence of CG31045-F (1–4373): upstream primer, ATTATCGGTCCGATGTTCCTCAAGCCGAA; downstream primer, ATCTCGTCCAGTTCTTCCTCCTGTTCCTT; 3′ sequence of CG31045-F (3990–5772): upstream primer, ACAGAAGATGACCAACGAGATGAACGATC; downstream primer, AATTAACTAGTCTATAATGCTTGTGCTGCTT. Each PCR product was ligated into the pCR4-TOPO vector (Invitrogen) with subsequent double restriction digestion using RsrII and EcoRI to ligate the 3′ sequences into pFastBac1 (Invitrogen) containing a C-terminal FLAG tag (DYKDDDDK) between the NotI and XbaI sites (pFastBac1-NX) followed by double digestion with EcoRI and SpeI to add in the 5′ sequences. Subsequent cloning of MMD fragments from full-length sequences utilized the QuikChangeII site-directed mutagenesis kit (Stratagene, Agilent Technologies, Santa Clara, CA) with sense and corresponding antisense primers designed to introduce an SpeI restriction site into the myosin-18 sequence that corresponds to residue Arg^{761} of *Dictyostelium* myosin-2 to generate a construct equivalent to a characterized minimal motor domain (18): M-PDZ (isoform A, 3957) sense primer, ACTAGTAGTACGTCGCGCTTGGCTT; M-ΔPDZ (isoform F, 3248) sense primer, ACTAGTAGCAGTACGTCGCGTTTAGCT. Double digestion of correctly sequenced positive mutant clones using EcoRI and SpeI was used for ligation into pFastBac1-NX.

Baculoviral Expression of MMD—Both MMD constructs were expressed in the baculoviral/Sf9 system. Infected cells were harvested by sedimentation after 48 h of growth. Cell pellets were quickly frozen in liquid nitrogen and either processed immediately or stored at −80 °C for processing later. Purification of myosin-18 proteins using the C-terminal FLAG tag was performed according to Wang *et al.* (19) except that 2 ml of FLAG resin (Invitrogen) was rotated with the cell lysate for 2 h at 4 °C, fractions were analyzed by 4–20% Tris-glycine SDS-PAGE, and fractions containing protein were pooled and dialyzed three times overnight against 1 liter of buffer containing 0.5 M KCl, 10 mM MOPS (pH 7.2), 0.1 mM EGTA, 3 mM NaN_3, 1 mM dithiothreitol (DTT), and 0.1 mM PMSF.

Characterization of Nucleotide Interaction—The actin-activated MgATPase activity of the myosin-18-MMD proteins was assayed with an NADH-coupled assay at 25 °C in the presence of 0.5 μM motor and concentrations of actin ranging to 50 μM F-actin (20). The solutions used for these measurements included the following reagents: 50 mM KCl, 10 mM MOPS (pH 7.2), 2 mM $MgCl_2$, 0.15 mM EGTA, 2 mM ATP, 40 units/ml lactate dehydrogenase, 200 units/ml pyruvate kinase, 1 mM phosphoenolpyruvate, and 200 μM NADH. Changes in A_{340} were monitored using a Beckman DU640 spectrophotometer. The radiometric K^+-EDTA ATPase assay as described in Pollard and Korn (21) was performed in buffer containing 0.5 M KCl, 20 mM MOPS (pH 7.0), 2 mM EDTA, and 0.5 mM [γ-^{32}P]ATP (PerkinElmer Life Sciences).

The emission and excitation spectra of nucleotide analog 3′-(7-diethylaminocoumarin-3-carbonylamino)-3′-deoxy-ATP

[2] The abbreviations used are: RACE, rapid amplification of cDNA ends; deac, 3′-(7-diethylaminocoumarin-3-carbonylamino)-3′-deoxy; mant, *N*-methylanthraniloyl derivative of 2′-deoxynucleotide; SkHMM, skeletal muscle myosin-2 heavy meromyosin; MMD, minimal motor domain of myosin; Dd, *D. discoideum*; NMIIB, nonmuscle myosin IIB; Myo2, myosin-2.

(deac-amino-ATP) and -ADP in the presence and absence of myosin-18-MMD constructs (1 μM) were taken with a FluoroMax3 photon-counting spectrofluorometer (Horiba Jobin Yvon) with thermostated cell housing. The protein was clarified by sedimentation for 10 min at 100,000 $\times$ *g* in a Beckman TLA-100 rotor at 4 °C just prior to the analysis. Excitation spectra were taken using an emission wavelength of 430 nm, and emission spectra were taken using an excitation wavelength of 470 nm. The buffer conditions were 0.5 M KCl (25 mM KCl for myosin-5-S1–6IQ), 10 mM MOPS (pH 7.2), 3 mM $MgCl_2$, 1 mM EGTA, and 1 mM DTT at 20 °C.

Binding of *N*-methylanthraniloyl derivatives of 2′-deoxy-ATP (mant-ATP) and 2′-deoxy-ADP (mant-ADP) to myosin-18-MMD constructs was analyzed using a stopped-flow apparatus (Sf2001, KinTek Corp., Austin, TX) by excitation at 365 nm using a 400-nm long pass filter for emissions. The conditions were 50 mM KCl, 20 mM MOPS (pH 7.0), 5 mM $MgCl_2$, and 0.05 mM EGTA at 25 °C using 0.4 μM myosin-18-MMD and 5 μM mant-nucleotide analogs.

Steady-state fluorescence anisotropy measurements of mant-ATP at 0.5 μM were taken using a FluoroMax3 photon-counting spectrofluorometer (Horiba Jobin Yvon) with thermostated cell housing. Protein samples were clarified by sedimentation immediately prior to the measurements by spinning for 10 min at 100,000 $\times$ *g* in a Beckman TLA-100 rotor at 4 °C. Resulting protein concentrations used for anisotropy experiments were 1.96 μM myosin-18 M-PDZ, 2.63 μM myosin-18 M-ΔPDZ, and 6.1 μM nonmuscle myosin IIB (NMIIB) S1 as a control. Further control anisotropy measurements to control for viscosity effects were taken in the presence of 2 mM unlabeled ATP. Experiments with myosin-18 motors were performed in buffer containing 0. 5 M KCl, 10 mM MOPS (pH 7.2), 0.1 mM EGTA, 3 mM NaN_3, and 1 mM DTT. Calculation of steady-state anisotropy was done with the equation $r = I_{VV} - I_{VH}/I_{VV} + 2I_{VH}$ where I_{VV} and I_{VH} are the corrected parallel and perpendicular polarized intensities, respectively.

Filter binding assays utilized nitrocellulose membrane pre-equilibrated with buffer containing 0.25 M KCl, 10 mM MOPS (pH 7.2), 4 mM $MgCl_2$, 0.1 mM EGTA, and 1 mM DTT. The membrane was placed under vacuum and blotted in duplicate with 1 μM myosin-18-MMD or skeletal muscle myosin-2 heavy meromyosin (SkHMM) preincubated with 20 μM [α-^{32}P]ATP (1.3×10^{15} cpm/mol) in the buffer mentioned above for 60 s. For quantification, dried membranes were exposed to Fujifilm BAS-MS phosphorimaging screens and scanned on a Fuji FLA-5000 series image analyzer (Fuji Medical Systems, Stamford, CT). Quantitation was done using Image Gauge software (version 3.0, Fuji Medical Systems).

Protein Unfolding Analysis—Circular dichroism (CD) spectra were recorded on a Jasco J720 spectropolarimeter equipped with a temperature controller using a 2-mm cuvette and wavelength range between 205 and 240 nm. All measurements were performed in buffer containing 0.5 M KCl, 10 mM KH_2PO_4 (pH 7.2), 0.1 mM EGTA, 3 mM NaN_3, and 1 mM DTT. For thermal denaturation experiments, the CD spectra were recorded after the protein samples were incubated for 5 min at different temperature points. Curves were analyzed with SigmaPlot 11.0.

Characterization of Actin Binding—Binding of myosin-18-MMD to F-actin was assayed by cosedimentation using 1 μM motor mixed with different concentrations of phalloidin-stabilized F-actin prepared from rabbit skeletal muscle (6) in the absence of ATP. Incubations were for 10 min at room temperature in buffer containing 0.1 M KCl, 20 mM MOPS (pH 7.0), 5 mM $MgCl_2$, 0.05 mM EGTA, 1 mM NaN_3, and 1 mM DTT. Variations on the cosedimentation assay included using 20 μM F-actin not stabilized by phalloidin, adding 1 mM ATP, and increasing incubation times of myosin-18 motor with F-actin up to 60 min. Following incubation, centrifugation at 100,000 $\times$ *g* in a Beckman TLA-100 rotor at 4 °C was performed. The supernatant was removed, and the pellet was resuspended in 1× SDS sample buffer to an equivalent volume. Supernatants and pellets were fractionated by 4–20% Tris-glycine SDS-PAGE. Gels were stained with Coomassie Blue and analyzed by densitometry (Odyssey version 3.0, Licor Biosciences, Lincoln, NE). Corresponding data points were fitted to a quadratic equation, correcting for the amount of motor that pellets itself in the absence of actin, typically in the range of 10% (SigmaPlot 11.0, Systat Software, Inc., San Jose, CA). For repeat pelleting assays, the supernatant from the first sedimentation at 20 μM actin was brought to the same actin concentration again, incubated as before, and then resedimented under the same assay conditions.

Actin Gliding Assays—Motility assays were performed in buffer containing 50 mM KCl, 20 mM MOPS (pH 7.4), 5 mM $MgCl_2$, 0.1 mM EGTA, 1 mM ATP, 25 μg/ml glucose oxidase, 45 μg/ml catalase, 2.5 mg/ml glucose, and 50 mM DTT. All experiments were performed at 30 °C with a 0.2 mg/ml total concentration of myosin. Noise within the motility setup was determined to be 0.066 ± 0.035 μm/s (n = 26) using 0.2 mg/ml SkHMM in the absence of ATP. Visualization of filaments and quantification of motility were performed in accordance with Homsher *et al.* (22).

Optical Trapping—Three-bead assays (23, 24) were performed using a dual beam optical trapping apparatus similar to that reported in Vanzi *et al.* (25) and Takagi and co-workers (26).

To perform the three-bead assay, an *in vitro* force assay chamber (volume, ~40 μl) was constructed using two coverslips, one of which was decorated sparsely with 2.1-μm-diameter glass microspheres (Bangs Laboratories, Fishers, IN) suspended in nitrocellulose, assembled using double sided adhesive tape. Myosin-18 motor constructs were diluted to a concentration of ~10–50 pM in 25 mM KCl, 25 mM imidazole, 4 mM $MgCl_2$, 1 mM EGTA (pH 7.4) at 22 °C (AB^- buffer) (27) and allowed to bind nonspecifically inside the chamber. Approximately 4 chamber volumes of AB^- buffer with 1 mg/ml bovine serum albumin were flushed through the chamber to reduce nonspecific binding of beads and actin filaments. AB^- buffer supplemented by the following reagents (2 mM creatine phosphate, 50 mM DTT, 10 μM ATP, 0.1 mg/ml creatine phosphokinase, 3 mg/ml glucose, 0.1 mg/ml glucose oxidase, and 0.02 mg/ml catalase; Ref. 28) was used in the final mixture together with 0.2 nM rhodamine-phalloidin (Invitrogen)-labeled, 10% biotinylated filamentous actin and NeutrAvidin (Thermo Fisher Scientific, Rockford, IL)-coated 1-μm biotin-labeled

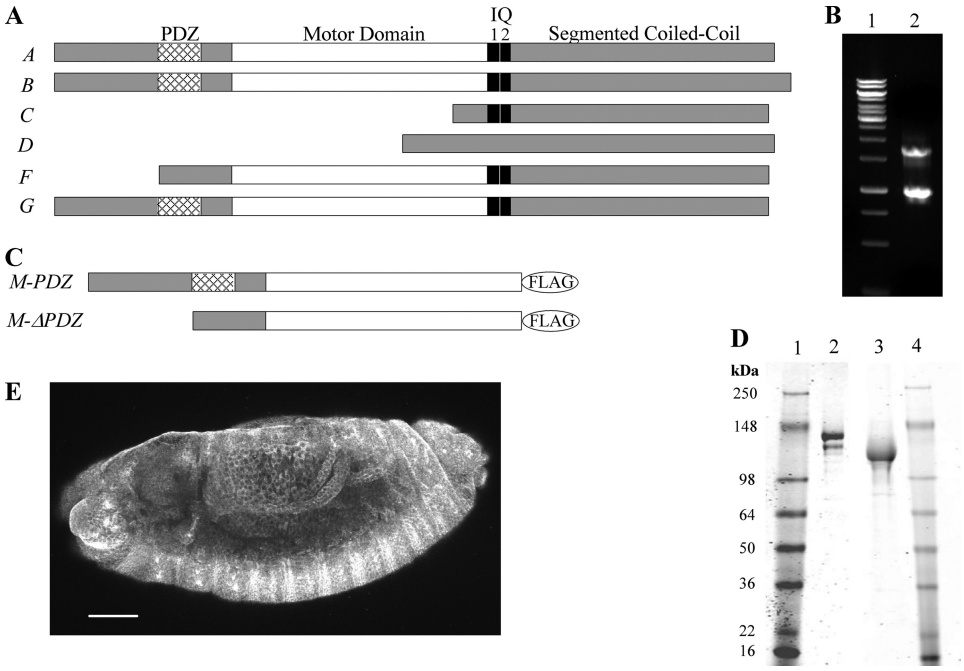

FIGURE 1. **Sequence analysis of PDZ and ΔPDZ isoforms of *Drosophila* myosin-18.** *A*, sequence analysis of 17 exons in the *Drosophila* myosin-18 gene (CG31045) was performed using the ClustalW multiple alignment algorithm. The domain analysis using Simple Modular Architecture Research Tool (SMART) at European Molecular Biology Laboratory was aligned with exons to illustrate six alternatively spliced isoforms (*A–G*) varying at the N terminus. *B*, *lane 1* is molecular weight standards. *Lane 2*, 5′ RACE analysis of whole fly mRNA using nested PCR to amplify PDZ and ΔPDZ isoforms yielded two bands, one at 1.7 kb corresponding to PDZ-containing isoforms and one at 0.9 kb corresponding to the ΔPDZ isoform. *C*, expression constructs of minimal motors of *Drosophila* myosin-18 for baculoviral expression in Sf9 cells truncate the sequence at Leu^{1319} for M-PDZ and Leu^{1082} for M-ΔPDZ, the residues corresponding to *Dictyostelium* myosin-2 Arg^{761}, followed by a C-terminal FLAG tag for purification. *D*, M-PDZ and M-ΔPDZ expressed proteins purified using a FLAG affinity tag and fractionated by 4–20% Tris-glycine SDS-PAGE. *Lane 1*, molecular weight markers; *lane 2*, M-PDZ at 140 kDa; *lane 3*, M-ΔPDZ at 116 kDa: *lane 4*, molecular weight markers. *E*, representative *Drosophila* embryo (stage 13) stained with a polyclonal antibody at a 1:1,000 dilution in blocking buffer (*scale bar*, 50 μm). The primary antibody was raised in rabbit against an uninterrupted segment of the coiled coil region of myosin-18 that is shared between all six potential isoforms of the protein. Visualization of the localization pattern used Alexa Fluor 488 goat anti-rabbit secondary antibody at a 1:5,000 dilution in blocking buffer. Using confocal microscopy with a 20×, 0.75 numerical aperture oil immersion objective and a section depth of 1.2 μm, the localization of myosin-18 was ubiquitous throughout all embryonic tissues as seen in this projection of 17 confocal sections. Such ubiquitous staining was seen throughout all observed embryonic developmental stages.

polystyrene beads conjugated with tetramethylrhodamine B-isothiocyanate (TRITC-BSA) (29). Thus, under fluorescence imaging, a single actin filament was attached to two 1-μm beads via manipulation of the optical traps. These bead/actin dumbbells (length, ~5–7 μm) were made taut and positioned above the glass microspheres attached to the surface of the chamber, functioning as a pedestal, to record transient unitary actomyosin-18 interactions. Only one of 15–20 pedestals exhibited unitary actomyosin interactions, providing statistical support for the concept that only a single myosin-18 motor was capable of interacting with the actin filament at any instance.

Experiments were performed using an optical trap stiffness of ~0.015–0.02 pico-newton/nm. Similar to experiments reported in Baboolal *et al.* (26), data were sampled at 20 kHz while sine waves (frequency, 200 Hz) of amplitudes of ~300 nm (peak to peak) were applied to one of the optical traps (30, 31). A decrease in the standard deviation of the noise level of this sine wave was used to distinguish regions of the collected data as periods either with or without myosin-18 motor attachments. Analysis was performed using custom software written in LabVIEW 6.0 (National Instruments, Corp., Austin, TX), and histograms were plotted using SigmaPlot 11.0 (Systat Software, Inc.). Histograms for both myosin-18 isoforms are compiled from data collected from five pedestals for M-PDZ ($n_{\text{myosin}} = 5$) and seven pedestals for M-ΔPDZ ($n_{\text{myosin}} = 7$).

Structural Comparison—The alignment of sequences of *Dictyostelium* myosin-2 (NCBI Reference Sequence accession number XM_632648) with *Drosophila* myosin-18 (CG31045-A) was performed with ClustalW (European Molecular Biology Laboratory). The crystal structure of *Dictyostelium discoideum* (Dd) myosin-2 (Protein Data Bank code 1MMD) was manipulated with ProteinWorkshop (version 3.8, Molecular Biology Toolkit; Ref. 32) to reflect residue insertions in myosin-18.

RESULTS

Genomic Analysis, Protein Expression, and Embryo Staining—Genome analysis of the *Drosophila* myosin-18 gene (CG31045) suggests the possibility of six alternatively spliced isoforms (Fig. 1*A*). The longest isoforms contain an N-terminal PDZ domain followed by a myosin motor domain, two IQ consensus sequences, and a long segmented coiled coil. There is no sequence homologous to the KE-rich region found in some mammalian myosin-18A isoforms. Shorter alternatively spliced *Drosophila* isoforms within the gene are truncated from the N terminus, producing isoforms lacking the PDZ domain or motor domain. All six isoforms share a conserved sequence within the tail region with the exception of their last exon, which distinguishes the longest isoforms from each other.

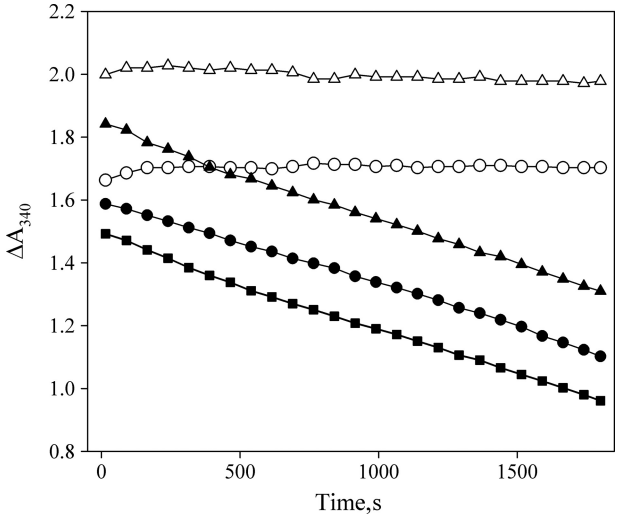

FIGURE 2. ***Drosophila* myosin-18 lacks actin-activated MgATPase activity.** M-PDZ and M-ΔPDZ were assayed for actin-activated MgATPase activity in an NADH-coupled assay. Representative traces of data from M-PDZ (○) and M-ΔPDZ (△) motors in the absence of actin show no detectable hydrolysis of ATP. In the presence of 45 μM F-actin and 2 mM ATP, M-PDZ (●) and M-ΔPDZ (▲) show no detectable difference in the rate of change of A_{340} from the ATP hydrolysis rate of actin alone (■) at the same concentration. Experiments were conducted at 25 °C in a buffer containing 50 mM KCl, 10 mM MOPS (pH 7.2), 2 mM $MgCl_2$, 0.15 mM EGTA, 2 mM ATP, 40 units/ml lactate dehydrogenase, 200 units/ml pyruvate kinase, 1 mM phosphoenolpyruvate, and 200 μM NADH. The concentration of myosin-18 fragments in each assay was 0.5 μM.

To date, mammalian myosin-18A isoforms have been classified as containing or lacking N-terminal PDZ domains. Thus, *Drosophila* myosin-18 PDZ and ΔPDZ isoforms were specifically targeted for analysis by 5′ RACE using a priming region within the motor domain (Fig. 1*B*). The cDNA sequence corresponding to both PDZ and ΔPDZ isoforms is present in whole fly mRNA extract. Antibody staining of *Drosophila* embryos using a polyclonal antibody capable of recognizing all six potential isoforms through the shared coiled coil sequence illustrates a ubiquitous staining pattern throughout embryos (Fig. 1*E*) and was seen at all embryonic developmental stages (data not shown).

Drosophila Myosin-18 Has No ATPase Activity—To analyze the PDZ and ΔPDZ isoforms kinetically, each isoform was expressed in an Sf9 baculoviral system as a minimal motor domain construct containing the respective N-terminal sequence and terminating with Leu^{1319} in M-PDZ and Leu^{1082} in M-ΔPDZ, the residues corresponding to Arg^{761} of *Dictyostelium* myosin-2 that constitutes a minimal catalytic domain for the myosin motor (18, 33) (Fig. 1*C*), along with a C-terminal FLAG affinity tag for purification. Successfully purified motor constructs were confirmed with gel electrophoresis and Western blotting against the FLAG epitope with the PDZ isoform running at 140 kDa and the ΔPDZ isoform running at 116 kDa as expected based on sequence analysis (Fig. 1*D*).

The two myosin-18 motor fragments were analyzed for the ability to hydrolyze ATP in an ATP-regenerating NADH-coupled actin-activated ATPase assay (Fig. 2). There was no detectable MgATP hydrolysis activity for either MMD construct in the absence of actin. Neither construct exhibited an activation of the MgATPase activity in the presence of actin compared with that of the actin alone. The actin concentration in these experiments ranged up to 50 μM actin with 2 mM ATP (data not shown). Further experiments determined that there was no detectable release of the P_i in a radiometric basal K^+-EDTA ATPase assay (21) (data not shown).

Three approaches were used to examine whether the MMD constructs were able to bind ATP. First, the fluorescent ATP analog deac-amino-ATP was used. The fluorescence intensity of this analog is typically enhanced upon binding to myosins (34, 35). The fluorescence intensity of deac-amino ATP showed no increase in the presence of the myosin-18 constructs (Fig. 3, *A* and *B*). In contrast, the fluorescence intensities of the same nucleotide increased 20-fold in the presence of myosin-5-S1–6IQ (Fig. 3, *C* and *D*) as has been shown previously (34). Similar results were seen using mant-ATP and mant-ADP, which showed no increase in the quantum yield in the presence of either isoform of *Drosophila* myosin-18 (36) (data not shown).

A second, more sensitive way to monitor nucleotide binding is to use fluorescence anisotropy. Here we compared the anisotropy values of mant-ATP alone with that of mant-ATP in the presence of *Drosophila* myosin-18 M-PDZ and -ΔPDZ proteins (Fig. 3*E*). As controls, we used NMIIB S1 and a control in which the proteins were first mixed with 2 mM ATP and then with mant-ATP to correct for any viscosity effects. The anisotropy value of the free mant-ATP was 0.018, which only increased minimally when *Drosophila* myosin-18 M-PDZ and -ΔPDZ proteins were added. In contrast, the anisotropy value of mant-ATP in the presence of NMIIB S1 was nearly 10-fold higher, indicating binding of the nucleotide to myosin. In the presence of excess unlabeled ATP, the anisotropy values of mant-ATP in the presence of NMIIB S1 or the myosin-18 proteins were in the same range as found for the *Drosophila* myosin-18 M-PDZ and -ΔPDZ proteins in the presence of mant-ATP alone.

Third, to more directly examine any potential binding of ATP to the myosin-18 nucleotide binding pocket, [α-^{32}P]ATP was used in a filter binding assay (Fig. 4). Subsequent phosphorimaging of the nitrocellulose membranes definitively showed that although a skeletal muscle myosin-2 heavy meromyosin control was able to bind radiolabeled ATP the *Drosophila* myosin-18 M-PDZ and -ΔPDZ proteins on the membrane showed only base-line levels of ATP. Collectively, these experiments provide strong evidence that *Drosophila* myosin-18 is unable to bind ATP.

CD Measurements and T_m Calculation—The results described above raised the question of whether the expressed myosin-18 protein is folded properly. To confirm the folding of the protein, the temperature-dependent unfolding of the proteins was analyzed using a CD spectrum of each construct.

Both *Drosophila* myosin-18 motor constructs unfolded in a single step between 40 and 50 °C (Fig. 5). The T_m measured for each construct with this method is in line with previously reported values from proteins in the myosin superfamily, which can range from 40 to 60 °C (37). Further confirmation of the proper folding of the *Drosophila* myosin-18 expressed proteins was provided by the change in tryptophan fluorescence over the same temperature range used in the CD measurements, which confirmed T_m values for the *Drosophila* myosin-18 proteins to be between 40 and 50 °C (data not shown).

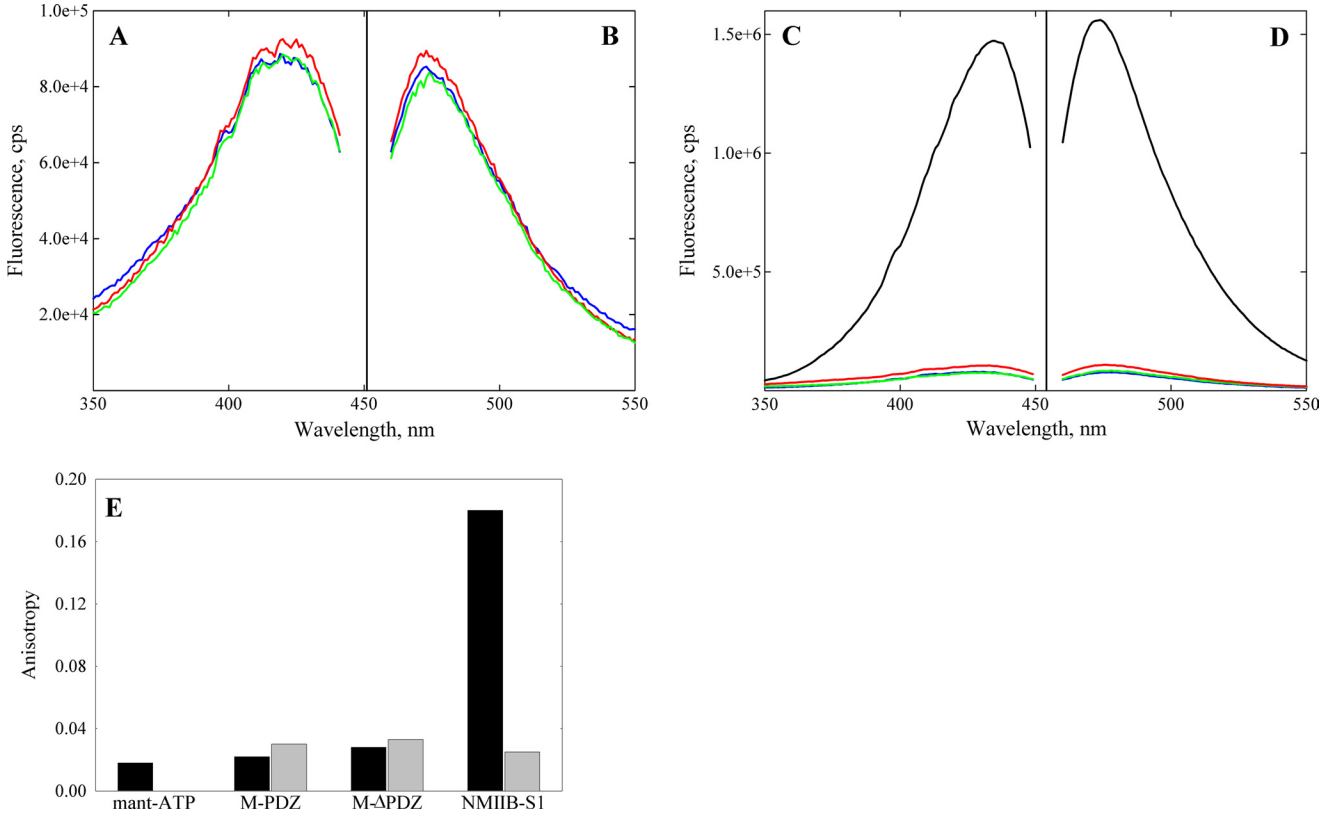

FIGURE 3. **Excitation and emission spectra of deac-amino nucleotides in presence and absence of myosin-18.** Excitation (*A*) and emission (*B*) spectra of deac-amino-ATP in binding assays using expressed M-PDZ (*red*) and M-ΔPDZ (*green*) in comparison with base-line fluorescence of the deac-amino moiety (*blue*) are shown. Fluorometric analysis of fluorescence signals from the deac moiety exhibited peak excitation at 430 nm and emission at 470 nm at 20 °C. Assays used 1 μM M-PDZ or M-ΔPDZ and 0.5 μM deac-amino-ATP in 0.5 M KCl, 10 mM MOPS (pH 7.2), 3 mM $MgCl_2$, 1 mM EGTA, and 1 mM DTT. The proteins were spun for 10 min at 100,000 × *g* in a Beckman TLA-100 rotor at 4 °C just prior to the assay to remove aggregates. *C* and *D*, excitation and emission spectra of deac-amino-ATP assays repeated and contrasted with 1 μM mouse myosin-5-S1–6IQ (*black*). Myosin-5-S1–6IQ was analyzed in a similar buffer as above but containing 25 mM KCl. Note the difference in the scale values for the fluorescence intensities in the two experiments. *E*, steady-state fluorescence anisotropy values comparing mant-ATP at 0.5 μM (*black*) alone in solution with mant-ATP in the presence of *Drosophila* myosin-18 M-PDZ and -ΔPDZ proteins at 1.96 and 2.63 μM, respectively. Experiments were performed in buffer containing 0. 5 M KCl, 10 mM MOPS (pH 7.2), 0.1 mM EGTA, 3 mM NaN_3, and 1 mM DTT. Controls using 6.1 μM NMIIB S1 and further controls for viscosity effects by adding 2 mM unlabeled ATP (*gray*) are also shown. *cps*, counts/s.

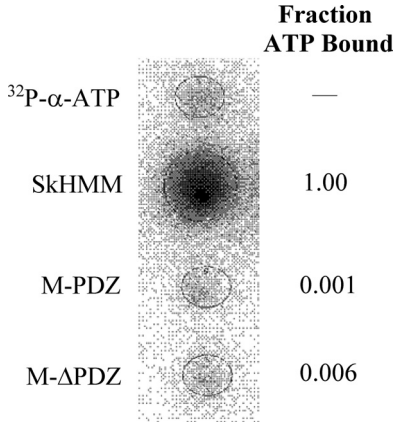

FIGURE 4. **Binding of [α-^{32}P]ATP to myosin via filter binding assay.** Rabbit SkHMM, M-PDZ, and M-ΔPDZ at 1 μM were incubated with 20 μM [α-^{32}P]ATP (1.3×10^{15} cpm/mol) for 60 s and blotted onto a nitrocellulose membrane pre-equilibrated with buffer containing 0.25 M KCl, 10 mM MOPS (pH 7.2), 0.1 mM EGTA, 3 mM NaN_3, and 1 mM DTT under vacuum. Blots of 20 μM [α-^{32}P]ATP (1.3×10^{15} cpm/mol) were used as controls. Following a rinse with excess equilibration buffer, the membrane was dried and exposed to Fujifilm BAS-MS phosphorimaging screens for 1 h. The fraction of [α-^{32}P]ATP bound to M-PDZ and M-ΔPDZ was calculated in relation to SkHMM after correcting for the amount of nucleic acid that binds nitrocellulose in the absence of protein.

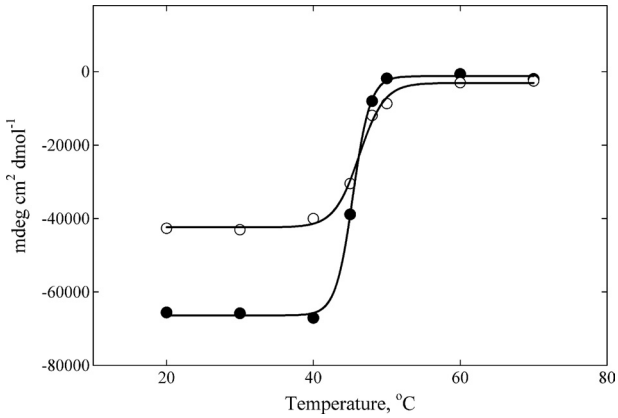

FIGURE 5. **CD spectrum of temperature-dependent unfolding of *Drosophila* myosin-18 proteins.** Data were collected at 222 nm over a range of temperatures determined at T_m = 45.4 ± 0.1 °C for M-PDZ (●) and T_m = 46.3 ± 0.3 °C M-ΔPDZ (○). Both proteins were dialyzed into buffer containing 0.5 M KCl, 10 mM KH_2PO_4 (pH 7.2), 0.1 mM EGTA, 3 mM NaN_3, and 1 mM DTT prior to the assay. The final concentration of M-PDZ used in the assay was 1.78 μM, and that of M-ΔPDZ was 2.85 μM. *mdeg*, millidegrees.

Myosin-18 Motor Binds to Actin in ATP-insensitive Manner—Both *Drosophila* myosin-18 motor constructs bound to F-actin in cosedimentation assays, and the binding of each became saturated below 100% even at high actin concentrations (Fig. 6*A*).

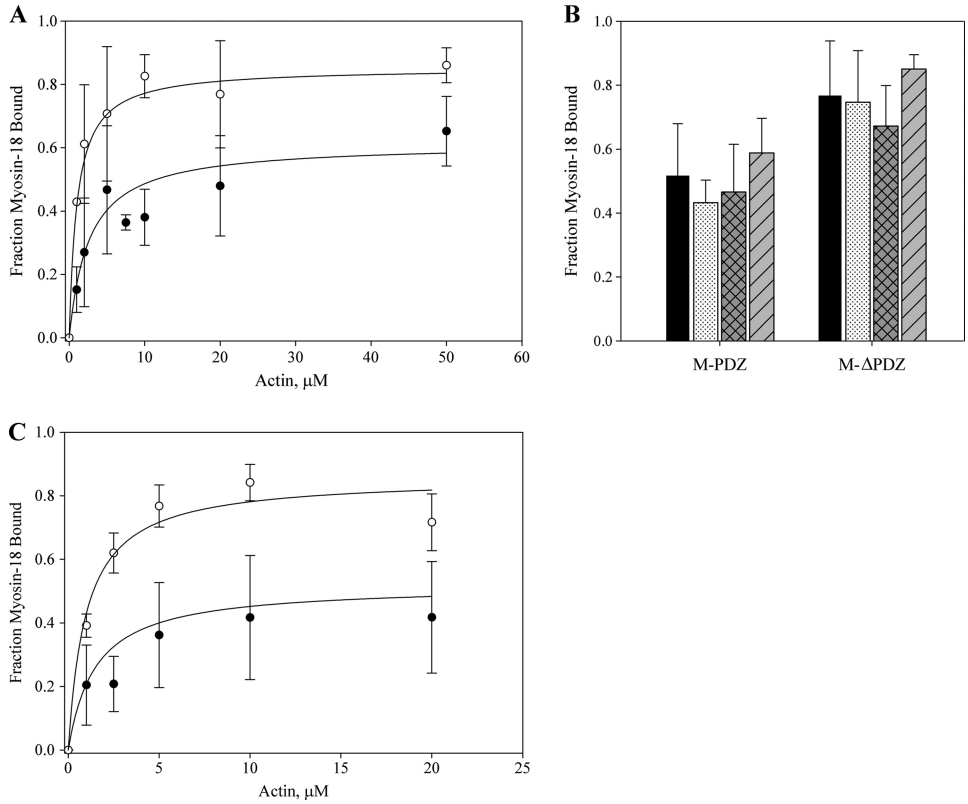

FIGURE 6. **Binding of myosin-18 isoforms to actin.** *A*, *Drosophila* myosin-18 motor constructs at a final concentration of 1 μM in buffer containing 0.1 mM KCl, 20 mM MOPS (pH 7.0), 5 mM $MgCl_2$, 0.05 mM EGTA, 1 mM NaN_3, and 1 mM DTT were incubated for 10 min at room temperature with increasing concentrations of phalloidin-stabilized F-actin in the absence of ATP. Reactions were sedimented at 100,000 $\times$ *g* for 15 min. Pellets and supernatants were separated by SDS-PAGE, and gels were stained and imaged with Coomassie Blue. Fractions of motor pelleted for each reaction were calculated by densitometry, correcting for the amount of motor that pellets itself in the absence of actin, typically in the range of 10%, for each preparation of protein. The fraction of myosin-18 motor bound was plotted against the concentration of actin introduced in each reaction. Data collected from M-PDZ (●) defined a K_d of 2.6 $\pm$ 0.2 μM and saturation at 58.2 $\pm$ 11.0%. Data from M-ΔPDZ (○) resulted in a K_d of 1.0 $\pm$ 0.2 μM and saturation at 83.2 $\pm$ 5.4%. The data represent multiple rounds of binding experiments using at least six different preparations of purified motor constructs for data collection. *Error bars* represent standard deviation of the mean (mean $\pm$ standard deviation). *B*, comparison of variations in the cosedimentation assay using M-PDZ and M-ΔPDZ. Cosedimentations at 20 μM actin in *A* (■) were compared with variations of the parameters within the cosedimentation assay, including the absence of phalloidin (▨), the presence of 1 mM ATP (▨), and 60-min incubation (▨). All variations were done at 20 μM actin with results showing no significant effect of any parameter on the myosin saturation curve. *C*, the effect of ATP on actin binding was further investigated with a range of actin titrations as in *A* in the presence of 1 mM ATP. Data collected from M-PDZ (●) in the presence of ATP gave a K_d of 1.5 $\pm$ 0.1 μM and saturation at 48.2 $\pm$ 14.5%. Data from M-ΔPDZ (○) resulted in a K_d of 1.0 $\pm$ 0.1 μM and saturation at 81.3 $\pm$ 8.9%. Conditions were as described in *A* except for the inclusion of 1 mM ATP.

Dissociation constants (K_d) determined by fitting the binding curves to a quadratic equation were determined to be 1.0 $\pm$ 0.2 μM with saturation at 83.2 $\pm$ 5.4% for M-ΔPDZ and 2.6 $\pm$ 0.2 μM with saturation at 58.2 $\pm$ 11.0% for M-PDZ. To further explore the nature of the lack of complete binding of myosin-18 motor to actin, variations on the cosedimentation protocol were carried out at 20 μM actin (Fig. 6*B*). Saturation consistent with the data presented for each motor in phalloidin-stabilized actin filaments in Fig. 6*A* was seen with untreated actin filaments. Varying the incubation period of myosin-18 motors with actin to 60 min (at room temperature) and 24 h (on ice) before sedimentation did not change the extent of motor bound. There are at least two possibilities to explain this saturable fractional binding of myosin-18-MMD to actin. It is possible that there is a fraction of the protein (40–50% for M-PDZ and 15–25% for M-ΔPDZ) that is denatured or improperly folded that cannot bind actin. Alternatively, there may be an equilibrium between a conformation that was competent to bind actin and a conformation that was incompetent to do so that is established within the time course of the sedimentation experiment.

To distinguish between these possibilities, the supernatant from the first sedimentation at 20 μM actin was brought to the same actin concentration again, incubated as before, and then resedimented. Of the protein remaining in the supernatant after the first sedimentation using M-PDZ, 50.3% rebound to actin in the second sedimentation, suggesting that there is an equilibrium between a binding-competent and a binding-incompetent conformation (Fig. 7). A similar equilibrium was observed for the myosin-18 M-ΔPDZ (data not shown) as well as with other myosins (6, 38).

Additionally, binding curves for both constructs were established in the presence of 1 mM ATP (Fig. 6*C*). Fitting those data to a quadratic equation revealed dissociation constants similar to those determined in the absence of ATP (1.0 $\pm$ 0.1 μM and saturation at 81.3 $\pm$ 8.9% for M-ΔPDZ and 1.5 $\pm$ 0.1 μM and saturation at 48.2 $\pm$ 14.5% for M-PDZ). These results further support our data suggesting that there is an ATP-insensitive F-actin binding property for myosin-18.

To explore the nature of the interaction of myosin-18 motor with actin, two approaches were used. We tested its ability to impede the translocation of actin filaments by an actively

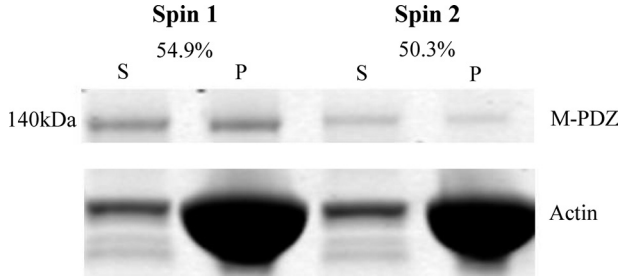

FIGURE 7. **Evidence for two conformational states of myosin-18 motor.** Myosin-18-MMD proteins were sedimented with 20 μM actin as in Fig. 6. The *left two lanes* show the supernatant (*S*) and pellet (*P*) fractions from a representative experiment using M-PDZ. The supernatant from this experiment was mixed with 20 μM actin, and a second sedimentation was performed. The supernatant and pellet from this experiment are shown in the *right two lanes*. The fraction of actin bound in the first sedimentation was 54.9%, and the fraction bound in the second sedimentation was 50.3%. Ionic conditions were as described in Fig. 6.

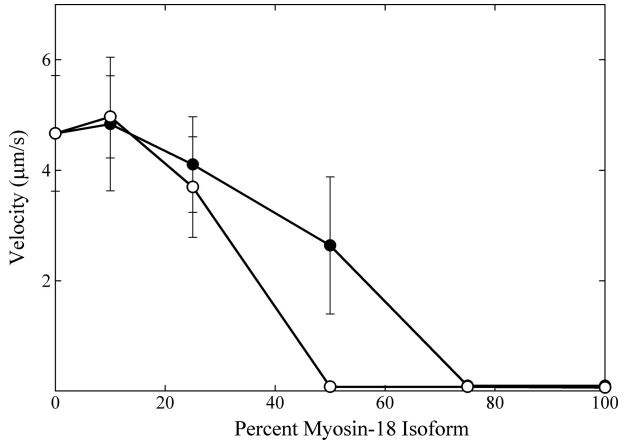

FIGURE 8. **Attenuation of skeletal muscle myosin-2 heavy meromyosin *in vitro* motility by *Drosophila* myosin-18.** Varying ratios of rabbit skeletal muscle myosin-2 heavy meromyosin to M-PDZ (●) or M-ΔPDZ (○) were mixed together with the total myosin concentration held constant at 0.2 mg/ml. Motility was assayed at 30 °C in buffer containing final concentrations of 50 mM KCl, 20 mM MOPS (pH 7.4), 5 mM $MgCl_2$, 0.1 mM EGTA, 1 mM ATP, 25 μg/ml glucose oxidase, 45 μg/ml catalase, 2.5 mg/ml glucose, and 50 mM DTT. Centroid tracking of at least 15 filaments was performed and analyzed with the CellTrak program. Noise within the motility setup was determined to be 0.066 ± 0.035 μm/s (n = 26) by imaging immobile actin filaments bound to a surface coated with 0.2 mg/ml SkHMM in the absence of ATP.

cycling myosin, SkHMM, in an *in vitro* motility assay. Previous studies showed that either actin-binding proteins or unphosphorylated smooth muscle myosin, which cannot move actin filaments, can retard and even stop the movement of actin filaments by SkHMM when mixed with this myosin on the coverslip surface (39, 40). Mixing increasing molar ratios of *Drosophila* myosin-18 motor constructs with SkHMM resulted in a slowing of the rate of movement of the actin filaments to the point where the movement eventually ceased (Fig. 8). M-PDZ halted SkHMM motility when the total myosin in the assay contained 75% myosin-18, whereas M-ΔPDZ was able to halt SkHMM motility with as little as 50% of the total myosin composition, consistent with the differences in binding affinities of the two motor constructs. When present on the coverslip surface alone, either of the *Drosophila* myosin-18 motor constructs tethered actin filaments to the surface but did not translocate them (data not shown).

The interaction of *Drosophila* myosin-18 motor constructs with actin was further explored using optical trapping in a three-bead assay. In this assay, an actin filament was tethered between two beads held by separate optical traps under an induced oscillation of 200 Hz, and the interaction of actin with motor bound to a larger surface bead was measured. Interactions between the myosin-18 motor and actin were detected by a decrease in the Brownian noise of the beads. Each interaction between *Drosophila* myosin-18 and actin was characterized for displacement. Both the M-PDZ and -ΔPDZ proteins interacted with actin within the assay (Fig. 9, *A* and *B*, respectively). Detachment rates were determined from fitting a single exponential fit to the respective histograms of lifetimes of *Drosophila* actomyosin-18 interactions (Fig. 9, *C* and *D*). The lifetimes for both constructs were brief with detachment rates of 94.2 ± 1.0 s^{-1} for M-PDZ and 57.0 ± 0.6 s^{-1} for M-ΔPDZ. Furthermore, displacement histograms for both constructs during the *Drosophila* actomyosin-18 interactions (Fig. 9, *E* and *F*) were centered at ~0 nm, suggesting that the protein does not induce a power stroke against the filament even in the presence of 10 μM ATP. For a mechanically active myosin, the displacement histogram will show a "shift" in the peak of the Gaussian distribution by the size of its power stroke as shown in previous studies (26, 30). Optical trapping data of both myosin-18 motor constructs provide further evidence that this myosin binds to actin but does not function as a typical actively cycling molecular motor.

DISCUSSION

The myosin superfamily is composed of 36 known classes as determined by sequence homology of the motor domain (1). Despite the high homology in amino acid sequence of the motor domains, there are considerable quantitative differences in rate constants of the individual steps in the enzymatic cycles, in the rate of *in vitro* motility, and in the strength of actin binding among the various myosins (41, 42). For example, the actin-activated MgATPase rate and the rate of translocation of actin filaments for nonmuscle myosin-2B was more than 100-fold less than that of fast skeletal muscle myosin (43). In addition, some myosins have high duty ratios and can move processively along actin as single molecules, whereas others cannot (34, 42). These differences in enzymatic properties along with extreme variations in the domain structure of the tail regions allow myosins to perform very diverse tasks within cells.

Drosophila myosin-18 represents the most extreme example of this motor diversity because it does not bind ATP but still retains the ability to bind to actin. In this regard, it behaves qualitatively similar to *Limulus* myosin-3 (recently reclassified as class 21; Ref. 1), which also does not bind ATP (6). This suggests that some myosins may function as dynamic actin tethers and, in this regard, should be added to the extensive list of actin-binding proteins with diverse functions, such as controlling actin polymerization, localizing actin to various cellular compartments, and bundling actin filaments into various higher order structures (21). A similar theme of motor diversity has been proposed for the microtubule-binding protein Vik1, which appears to have evolved from a kinesin-14 motor to feature a tertiary structure resembling a motor-like fold but has

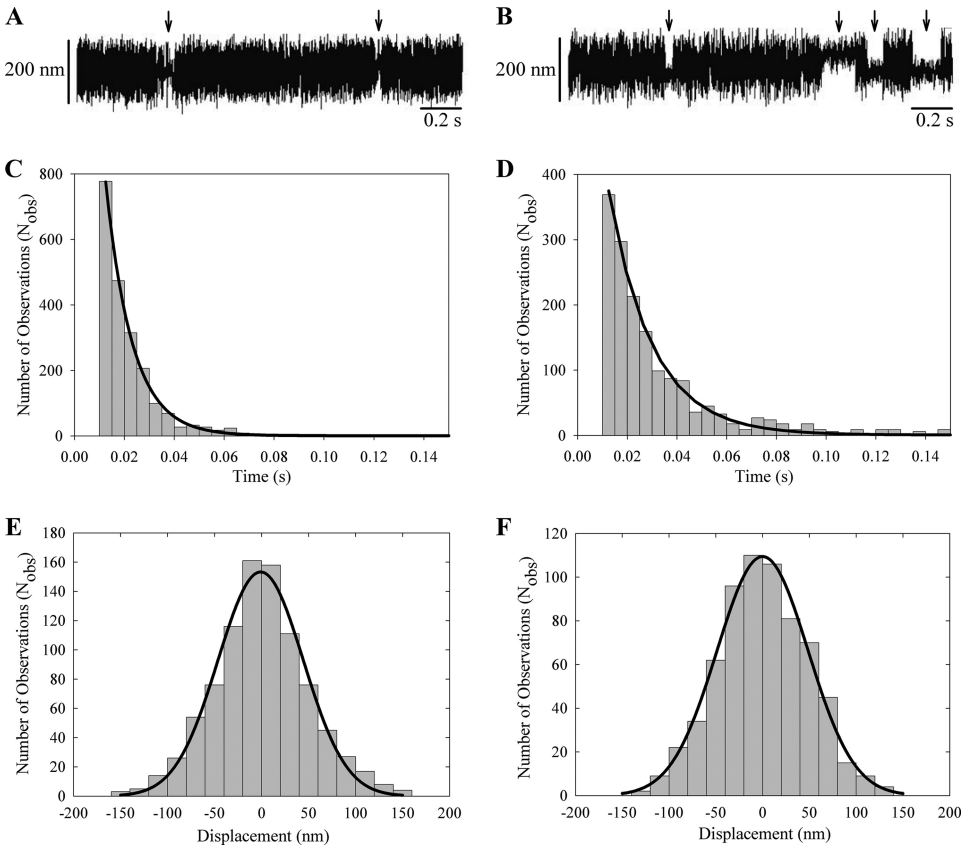

FIGURE 9. **Optical trapping analysis of single molecule interactions.** *A* and *B*, three-bead assays with oscillations show brief interactions between M-PDZ (*A*) or M-ΔPDZ (*B*) and rhodamine-phalloidin stabilized F-actin. *Arrows* point to attachment events. *C* and *D*, lifetime data of myosin-18 motor interactions longer than 10 ms collected in the optical trap were fitted to a single exponential curve. M-PDZ (*C*) yielded a detachment rate of 94.2 ± 1.0 s^{-1}, and M-ΔPDZ (*D*) yielded a detachment rate of 57.0 ± 0.6 s^{-1}. *E* and *F*, fitting the displacement data collected from the optical trap during each actomyosin-18 interaction to a Gaussian distribution yielded histograms centered at −0.98 ± 1.6 nm for M-PDZ (*E*) and at −0.03 ± 1.35 nm for M-ΔPDZ (*F*). Data were collected at 22 °C in a buffer containing 25 mM KCl, 25 mM imidazole (pH 7.4), 4 mM $MgCl_2$, 1 mM EGTA, 2 mM creatine phosphate, 50 mM DTT, 10 μM ATP, 0.1 mg/ml creatine phosphokinase, 3 mg/ml glucose, 0.1 mg/ml glucose oxidase, and 0.02 mg/ml catalase.

lost the loop and switch regions that are necessary for ATP binding (44).

Our minimal motor domain construct is truncated at Leu^{1319} in M-PDZ and Leu^{1082} in M-ΔPDZ, which corresponds to residue Arg^{761} of *Dictyostelium* myosin-2. Truncations of myosins beyond Ile^{754} of that motor have been shown to retain catalytic activity (18, 33). We would therefore expect our truncated constructs to reflect the full kinetic function of myosin-18 while eliminating the need for bound light chains that themselves may require modifications to elicit function of the motor.

We provide several lines of evidence to support the lack of nucleotide binding by myosin-18. These include lack of perturbation of the fluorescence intensity and anisotropy of mant-ATP and deac-amino-ATP, lack of interaction with [α-^{32}P]ATP, and lack of effect of ATP on the binding of myosin-18 to actin measured either by direct sedimentation assays or from the lifetimes of attached events in the optical trap.

We confirmed that this lack of nucleotide binding cannot be attributed to spurious amino acid substitutions within the cloned sequences because the sequence of the clones matches that in the database. Further supporting evidence that the lack of ATP binding is an inherent property of this motor and not a result of protein misfolding was established by CD spectrum and tryptophan fluorescence analyses of temperature-dependent unfolding of each molecule. We established T_m values for the myosin-18 proteins in the range of 40–50 °C, which is similar to those reported for other myosins (37), suggesting proper folding of our proteins.

The inherent lack of ATP binding could be attributed to several interesting residues found at integral sites in the amino acid sequence of the motor (Fig. 10*A*). The sequence of the P-loop of myosin-18 is fairly conserved from the standard myosin sequence (GRSGAGKS compared with the consensus GESGAGKT). The Switch I and II regions of myosin-18 do exhibit several differences from conserved motor sequences (N*X*NSSRFGK). In Switch I, two types of differences can be seen. First, there are residue changes substituting consensus amino acids with alternative residues that have bulkier side chains. These alterations, including Thr^{709} of *Drosophila* myosin-18 replacing a serine and Thr^{712} replacing a glycine, may affect the position of Switch I, thereby preventing its role in coordinating potential bound nucleotide and Mg^{+2} or preventing the binding of nucleotide altogether. Second, residues known to be important in the transition between states during the kinetic cycle of the motor (Ala^{708} substituted for the consensus serine) are altered from the conserved sequence. Although these changes may not explain a total lack of nucleotide binding, other reports suggest that these mutations would be

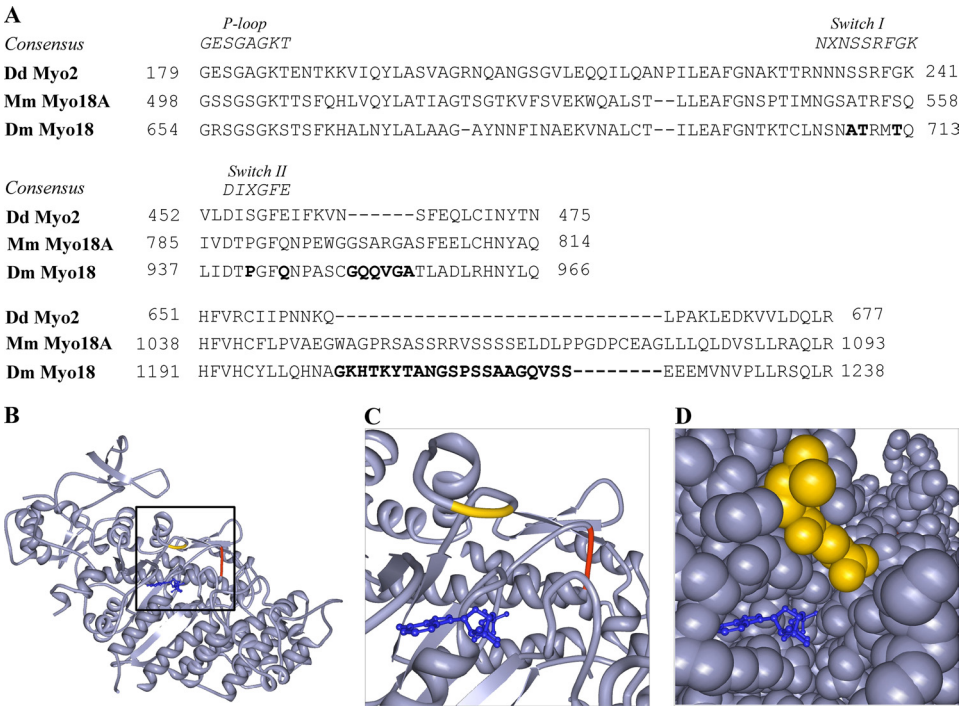

FIGURE 10. **Unique amino acid sequence features of *Drosophila* myosin-18.** *A*, sequence alignments of amino acid residues from the P-loop, Switch I (*upper alignment*), and Switch II (*middle alignment*) regions of *Drosophila* myosin-18 in comparison with consensus sequences from these regions and sequences from motor domains of Dd Myo2 and *Mus musculus* myosin-18A (*Mm myo18A*). The *lower alignment* demonstrates the presence of a 21-residue insertion for *D. melanogaster* myosin-18 (*Dm Myo18*) and a 29-residue insertion for *Mus musculus* myosin-18A between the region bounded by amino acids Gln^{662} and Leu^{663} in Dd Myo2. Alignments also reveal amino acid insertions in multiple locations, including a 6-residue insertion between Dd Myo2 residues Asn^{464} and Ser^{465}. *Bold residues* are discussed in the text. *B* and *C*, using ribbon diagrams of the crystal structure of the motor domain of Dd Myo2 (Protein Data Bank code 1MMD; ADP, *blue*), the two *D. melanogaster* myosin-18 amino acid extensions in *A* are illustrated by highlighting the flanking Dd Myo2 amino acids. The 6-residue insertion between Dd Myo2 Asn^{464} and Ser*465* (*red*) is located at the end of Switch II, whereas the 21-residue insertion between Gln^{662} and Leu^{663} (*yellow*) is located before the SH2 helix of the motor. *D*, space-filling model of the crystal structure of the same region as in *C*. The Gln^{662}-Leu^{663} insertion can be seen on the surface of the motor, suggesting it to be a large surface loop that may potentially change how rearrangements of the motor domain occur during the kinetic cycle. The Asn^{464}-Ser^{465} insertion, however, cannot be seen clearly in the space-filling model, suggesting that the 6-residue insertion would be buried within the motor structure and could potentially change the dynamics of cleft closure and perhaps produce a well defined motor structure with low nucleotide affinity and weakened affinity for actin.

expected to result in slower hydrolysis rates and slower P_i release (45).

Switch II (DI*X*GFE) of myosin-18 replaces a conserved glutamic acid with a glutamine (Gln^{944} of *Drosophila* myosin-18 isoform A). In other myosins, this glutamic acid forms a salt bridge with a conserved arginine in Switch I. Disrupting the salt bridge by mutating this glutamic acid has been shown in smooth muscle myosin or *Dictyostelium* myosin-2 to dramatically decrease the rate of basal and actin-activated nucleotide hydrolysis by the motor but does not interfere with the binding of nucleotide into the pocket (46–48). However, in the case of myosin-18 motors, the glutamic acid is mutated to a glutamine, and such a substitution may not prevent closure of Switch II but may instead destabilize the pre-power stroke conformation and instead favor a post-rigor conformation.

The presence of a proline in Switch II (Pro^{941} of *Drosophila* myosin-18 isoform A) could result in a restriction of the conformations that the flexible switch could adopt during the kinetic cycle of the motor. This proline residue would also affect the position of the nitrogen in the following glycine, which is integral for ATP binding and transitioning the switch to a pre-power stroke conformation.

In addition to these single residue substitutions in the myosin-18 motor, there are also two regions of extended amino acid insertions that we propose may also play a role in making this motor highly divergent from the superfamily (Fig. 10, *B–D*). A 6-amino acid extension after Switch II, between corresponding residues Asn^{464} and Ser^{465} in Dd Myo2, is likely buried within the interior of the motor domain. By comparison, other myosin amino acid insertions (compared with rabbit skeletal muscle myosin) are usually present in surface loops (49), whereas the lengths of the various helices and β-sheets in the "interior" of the myosin domain are generally well conserved. The added bulk from these inserted buried residues could potentially change the dynamics of the cleft closure of the motor, perhaps producing a well defined structure for the motor with low affinity for nucleotide and weakened affinity for actin (46, 48, 50). A second insertion of interest in the *Drosophila* myosin-18 sequence involves a 21-residue surface loop extension that precedes the SH2 helix of the motor, inserted between corresponding residues Gln^{662} and Leu^{663} in Dd Myo2. A similar insertion of 29 residues is present in *Mus musculus* myosin-18A. This long, flexible extension may potentially change how rearrangements of regions of the motor domain occur.

Another possibility is that the activity of *Drosophila* myosin-18 is regulated by some post-translational mechanism, such as a phosphorylation or the binding of a regulatory protein, and that we have isolated the myosin in an inactive state. However, other myosins that have been shown to be regulated, such as lower eukaryotic myosin-1, smooth muscle myosin-2, and

myosin-5, bind nucleotide and have low basal MgATPase activities in their "off" states (12, 39, 42). There is no precedent for a myosin regulatory mechanism at the level of nucleotide binding.

The affinity of *Drosophila* myosin-18 for actin is intermediate between that typically exhibited by other myosins in their nucleotide-free state (strong binding) and in the ATP-bound state (weak binding). The lack of stoichiometric binding observed was similar to that seen with *Limulus* myosin-3 (6) or with myosin-9 (38) in the presence of ADP and suggests that there may be an equilibrium between a conformation of myosin-18 that is competent to bind to actin and a conformation that does not bind to actin. In the case of all three of these myosins, it was found that addition of actin to the unbound fraction followed by another sedimentation resulted again in only partial binding of the myosin. We have not been able to establish a suitable kinetic model to explain both the partial binding of myosin-18 to actin in the first sedimentation and the partial binding seen in the subsequent resedimentation.

Drosophila myosin-18 bound to a coverslip surface is capable of tethering fluorescently labeled actin filaments. In addition, when mixed with skeletal muscle myosin on a coverslip surface, it can attenuate the rapid translocation of actin filaments exhibited by that myosin and, at higher ratios of myosin-18 to skeletal muscle myosin, can fully stop the movement of actin filaments. This supports the notion that myosin-18 dynamically binds to actin filaments as its behavior in this experiment mimics that of other actin-binding proteins, such as α-actinin and filamin (51). Furthermore, the transient binding of myosin-18 to actin can be seen in optical trapping experiments with no significant power stroke, consistent with myosin-18 functioning as a tethering protein rather than a motor protein. M-PDZ and M-ΔPDZ also exhibited slightly different detachment rates determined from optical trapping experiments. Perhaps the N-terminal extension of this myosin provides an alternate actin binding mechanism to that of the conventional actin binding via the motor domain. Using the detachment rates from the optical trapping experiments and the affinity constants determined from cosedimentation assays, we can estimate the apparent actin binding on-rate for this myosin to be in the range of $\sim$2–10 $\times$ 10^7 M^{-1} s^{-1}, which is similar to rates observed for other myosins (52, 53).

The affinity of myosin-18 for actin is in the 1 μM range like other actin-binding proteins, including α-catenin (54), talin (55), and α-actinin (56). This affinity is much lower than most members of the myosin superfamily when no nucleotide is present with the exception of *Limulus* myosin-3 whose affinity has been calculated to be 0.1 μM (6, 41). It is well known that bound ATP (or ADP·P_i) dramatically reduces the actin affinity for most myosins with no nucleotide bound (41).

The affinity of myosins for actin may be modulated by the degree of closure of the cleft between two large subdomains that constitute the actin interface in the head. Crystal structures of numerous myosins in the presence of different nucleotides show that this cleft can be in an open or closed conformation. Recent molecular modeling of myosin crystal structures into the density obtained from electron microscopic images of myosin motor domains bound to actin suggests that in the higher affinity, no nucleotide bound state the cleft is closed (50). The lower affinity of myosin-18 for actin suggests that the head conformation of myosin-18 is intermediate between that of the apo state and the nucleotide-bound state for typical myosins.

Only one study has been published on the biochemical properties of the mammalian myosin-18A protein (14). In that study, heavy meromyosin-like (two-headed) constructs of myosin-18A with and without the N-terminal extension were expressed in HeLa cells and used in actin cosedimentation assays without purification. Interestingly, the isoform containing the region between the KE-rich and the PDZ domains bound to actin in an ATP-insensitive manner, whereas constructs missing this region did not bind to actin under either condition. These data suggest that only the region between the KE-rich domain and the PDZ domain can interact with actin and that the mammalian myosin-18 motor domain, unlike that of *Drosophila*, does not interact with actin at all. No attempts were made to directly measure the ATPase activity or the nucleotide binding of these isoforms (14).

A recent study by Dippold *et al.* (11) suggested that mammalian myosin-18A interacts with the Golgi-associated protein GOLPH3 and participates in the maintenance of trans-Golgi structure. This study used siRNA knockdown of the endogenous myosin-18A and found that trans-Golgi structure was disrupted. Normal structure could be rescued by a wild-type myosin-18A construct but not by an ATPase mutant construct of myosin-18A corresponding to mutations in myosin-2 that abolish MgATPase activity in that myosin. This study suggests that the mammalian myosin-18A may have MgATPase activity, and the authors of the study speculate that the motor activity of this myosin is necessary for formation of proper Golgi structure. However, the conflicts between the above study (11) and the Isogawa *et al.* (14) study suggest the need for biochemical experiments to be conducted on purified mammalian myosin-18A before comparisons are made with the *Drosophila* myosin-18 protein.

The data reported here suggest that *Drosophila* myosin-18 does not have MgATPase activity, nor does it have the ability to bind ATP, but its motor domain, both with and without the N-terminal extension, does have the ability to bind and tether actin. The full-length protein is encoded to have a long segmented coiled coil in the tail region that may allow it to oligomerize into thick filaments similar to those formed by myosin-2. If so, these multiply aligned heads would dramatically increase the effective actin affinity of the complex and if the filaments were bipolar, such as those formed by nonmuscle myosin-2, could tether actin filaments of opposite polarity. *Drosophila* myosin-18 may also act as a protein scaffold to tether other proteins to actin. Some isoforms contain an N-terminal PDZ domain, which is a well known protein-protein interaction domain. From our studies, the PDZ domain does not appear to confer any kinetic changes within the motor. Future studies will seek to identify binding partners for the full-length molecule through the PDZ domain as well as through the tail.

Acknowledgments—We thank Fang Zhang for excellent technical assistance, Benjamin Lelouvier (Laboratory of Cell Biology, National Heart, Lung and Blood Institute, National Institutes of Health) for assistance with confocal microscopy, Grzegorz Piszczek (Biophysics Core Facility, National Heart, Lung and Blood Institute, National Institutes of Health) for advice and assistance on circular dichroism experiments performed in this study, and Kathryn Callahan (National Institute of Diabetes and Digestive and Kidney Diseases, National Institutes of Health) for technical assistance with filter binding assays. We thank Earl Homsher (University of California, Los Angeles), Mihaly Kovacs (Eotvos University, Budapest, Hungary), and Michael Geeves (University of Kent, Canterbury, UK) for discussions on possible kinetic mechanisms.

REFERENCES

1. Odronitz, F., and Kollmar, M. (2007) *Genome Biol.* **8,** R196
2. Furusawa, T., Ikawa, S., Yanai, N., and Obinata, M. (2000) *Biochem. Biophys. Res. Commun.* **270,** 67–75
3. Doyle, D. A., Lee, A., Lewis, J., Kim, E., Sheng, M., and MacKinnon, R. (1996) *Cell* **85,** 1067–1076
4. Nishioka, M., Kohno, T., Tani, M., Yanaihara, N., Tomizawa, Y., Otsuka, A., Sasaki, S., Kobayashi, K., Niki, T., Maeshima, A., Sekido, Y., Minna, J. D., Sone, S., and Yokota, J. (2002) *Proc. Natl. Acad. Sci. U.S.A.* **99,** 12269–12274
5. Ajima, R., Kajiya, K., Inoue, T., Tani, M., Shiraishi-Yamaguchi, Y., Maeda, M., Segawa, T., Furuichi, T., Sutoh, K., and Yokota, J. (2007) *Biochem. Biophys. Res. Commun.* **356,** 851–856
6. Kempler, K., Tóth, J., Yamashita, R., Mapel, G., Robinson, K., Cardasis, H., Stevens, S., Sellers, J. R., and Battelle, B. A. (2007) *Biochemistry* **46,** 4280–4293
7. Berg, J. S., Powell, B. C., and Cheney, R. E. (2001) *Mol. Biol. Cell* **12,** 780–794
8. Foth, B. J., Goedecke, M. C., and Soldati, D. (2006) *Proc. Natl. Acad. Sci. U.S.A.* **103,** 3681–3686
9. Yanaihara, N., Nishioka, M., Kohno, T., Otsuka, A., Okamoto, A., Ochiai, K., Tanaka, T., and Yokota, J. (2004) *Int. J. Cancer* **112,** 150–154
10. Nakano, T., Tani, M., Nishioka, M., Kohno, T., Otsuka, A., Ohwada, S., and Yokota, J. (2005) *Genes Chromosomes Cancer* **43,** 162–171
11. Dippold, H. C., Ng, M. M., Farber-Katz, S. E., Lee, S. K., Kerr, M. L., Peterman, M. C., Sim, R., Wiharto, P. A., Galbraith, K. A., Madhavarapu, S., Fuchs, G. J., Meerloo, T., Farquhar, M. G., Zhou, H., and Field, S. J. (2009) *Cell* **139,** 337–351
12. Tan, I., Yong, J., Dong, J. M., Lim, L., and Leung, T. (2008) *Cell* **135,** 123–136
13. Mori, K., Matsuda, K., Furusawa, T., Kawata, M., Inoue, T., and Obinata, M. (2005) *Biochem. Biophys. Res. Commun.* **326,** 491–498
14. Isogawa, Y., Kon, T., Inoue, T., Ohkura, R., Yamakawa, H., Ohara, O., and Sutoh, K. (2005) *Biochemistry* **44,** 6190–6196
15. Rio, D. C., Ares, M., Jr., Hannon, G. J., and Nilsen, T. W. (2010) *Cold Spring Harb. Protoc.* **2010,** pdb.prot5439
16. Harlow, E., and Lane, D. (2006) *Cold Spring Harb. Protoc.* **2006,** pdb.prot4525
17. Harlow, E., and Lane, D. (2006) *Cold Spring Harb. Protoc.* **2006,** pdb.prot4527
18. Kuhlman, P. A., and Bagshaw, C. R. (1998) *J. Muscle Res. Cell Motil.* **19,** 491–504
19. Wang, F., Harvey, E. V., Conti, M. A., Wei, D., and Sellers, J. R. (2000) *Biochemistry* **39,** 5555–5560
20. Trentham, D. R., Bardsley, R. G., Eccleston, J. F., and Weeds, A. G. (1972) *Biochem. J.* **126,** 635–644
21. Pollard, T. D., and Korn, E. D. (1973) *J. Biol. Chem.* **248,** 4682–4690
22. Homsher, E., Wang, F., and Sellers, J. R. (1992) *Am. J. Physiol. Cell Physiol.* **262,** C714–C723
23. Finer, J. T., Simmons, R. M., and Spudich, J. A. (1994) *Nature* **368,** 113–119
24. Molloy, J. E., Burns, J. E., Kendrick-Jones, J., Tregear, R. T., and White, D. C. (1995) *Nature* **378,** 209–212
25. Vanzi, F., Takagi, Y., Shuman, H., Cooperman, B. S., and Goldman, Y. E. (2005) *Biophys. J.* **89,** 1909–1919
26. Baboolal, T. G., Sakamoto, T., Forgacs, E., White, H. D., Jackson, S. M., Takagi, Y., Farrow, R. E., Molloy, J. E., Knight, P. J., Sellers, J. R., and Peckham, M. (2009) *Proc. Natl. Acad. Sci. U.S.A.* **106,** 22193–22198
27. Kron, S. J., and Spudich, J. A. (1986) *Proc. Natl. Acad. Sci. U.S.A.* **83,** 6272–6276
28. Kishino, A., and Yanagida, T. (1988) *Nature* **334,** 74–76
29. Rock, R. S., Rief, M., Mehta, A. D., and Spudich, J. A. (2000) *Methods* **22,** 373–381
30. Sakamoto, T., Wang, F., Schmitz, S., Xu, Y., Xu, Q., Molloy, J. E., Veigel, C., and Sellers, J. R. (2003) *J. Biol. Chem.* **278,** 29201–29207
31. Batters, C., Wallace, M. I., Coluccio, L. M., and Molloy, J. E. (2004) *Philos. Trans. R. Soc. Lond. B Biol. Sci.* **359,** 1895–1905
32. Moreland, J. L., Gramada, A., Buzko, O. V., Zhang, Q., and Bourne, P. E. (2005) *BMC Bioinformatics* **6,** 21
33. Woodward, S. K., Geeves, M. A., and Manstein, D. J. (1995) *Biochemistry* **34,** 16056–16064
34. Forgacs, E., Cartwright, S., Kovács, M., Sakamoto, T., Sellers, J. R., Corrie, J. E., Webb, M. R., and White, H. D. (2006) *Biochemistry* **45,** 13035–13045
35. Heeley, D. H., Belknap, B., and White, H. D. (2006) *J. Biol. Chem.* **281,** 668–676
36. Woodward, S. K., Eccleston, J. F., and Geeves, M. A. (1991) *Biochemistry* **30,** 422–430
37. Zolkiewski, M., Redowicz, M. J., Korn, E. D., and Ginsburg, A. (1996) *Biophys. Chem.* **59,** 365–371
38. Nalavadi, V., Nyitrai, M., Bertolini, C., Adamek, N., Geeves, M. A., and Bähler, M. (2005) *J. Biol. Chem.* **280,** 38957–38968
39. Sellers, J. R. (1985) *J. Biol. Chem.* **260,** 15815–15819
40. Harris, D. E., Work, S. S., Wright, R. K., Alpert, N. R., and Warshaw, D. M. (1994) *J. Muscle Res. Cell Motil.* **15,** 11–19
41. Sellers, J. R. (1999) *Myosins*, 2nd Ed., Oxford University Press, Oxford, UK
42. De La Cruz, E. M., and Ostap, E. M. (2004) *Curr. Opin. Cell Biol.* **16,** 61–67
43. Forgacs, E., Sakamoto, T., Cartwright, S., Belknap, B., Kovács, M., Tóth, J., Webb, M. R., Sellers, J. R., and White, H. D. (2009) *J. Biol. Chem.* **284,** 2138–2149
44. Allingham, J. S., Sproul, L. R., Rayment, I., and Gilbert, S. P. (2007) *Cell* **128,** 1161–1172
45. Shimada, T., Sasaki, N., Ohkura, R., and Sutoh, K. (1997) *Biochemistry* **36,** 14037–14043
46. Furch, M., Geeves, M. A., and Manstein, D. J. (1998) *Biochemistry* **37,** 6317–6326
47. Onishi, H., Morales, M. F., Kojima, S., Katoh, K., and Fujiwara, K. (1997) *Biochemistry* **36,** 3767–3772
48. Ruppel, K. M., and Spudich, J. A. (1996) *Mol. Biol. Cell* **7,** 1123–1136
49. Sellers, J. R., Goodson, H. V., and Wang, F. (1996) *J. Muscle Res. Cell Motil.* **17,** 7–22
50. Lorenz, M., and Holmes, K. C. (2010) *Proc. Natl. Acad. Sci. U.S.A.* **107,** 12529–12534
51. Janson, L. W., Sellers, J. R., and Taylor, D. L. (1992) *Cell Motil. Cytoskeleton* **22,** 274–280
52. Cremo, C. R., and Geeves, M. A. (1998) *Biochemistry* **37,** 1969–1978
53. De La Cruz, E. M., Wells, A. L., Rosenfeld, S. S., Ostap, E. M., and Sweeney, H. L. (1999) *Proc. Natl. Acad. Sci. U.S.A.* **96,** 13726–13731
54. Rimm, D. L., Koslov, E. R., Kebriaei, P., Cianci, C. D., and Morrow, J. S. (1995) *Proc. Natl. Acad. Sci. U.S.A.* **92,** 8813–8817
55. Hemmings, L., Rees, D. J., Ohanian, V., Bolton, S. J., Gilmore, A. P., Patel, B., Priddle, H., Trevithick, J. E., Hynes, R. O., and Critchley, D. R. (1996) *J. Cell Sci.* **109,** 2715–2726
56. Winder, S. J., Hemmings, L., Maciver, S. K., Bolton, S. J., Tinsley, J. M., Davies, K. E., Critchley, D. R., and Kendrick-Jones, J. (1995) *J. Cell Sci.* **108,** 63–71